Distributed Model-Free Adaptive Control Strategy for Hybrid AC/DC Microgrid With Event-Triggered Mechanism

Chang Yang, *Student Member, IEEE*, Tao Zheng, Ming Bu, Pengyu Li, and Josep M. Guerrero, *Fellow, IEEE*

***Abstract*—A distributed control strategy (DCS) is an efficient way to realize power sharing among distributed generators (DGs) and restore the voltage deviation caused by droop control. However, there are several limitations in the traditional strategy of hybrid ac/dc microgrid (MG), such as the heavy communication burden and sensitivity to the working conditions. In this article, a distributed model-free adaptive control strategy (DMFAC) is proposed with an event-triggered (ET) mechanism. A unified control framework of hybrid MG is established and the ET-DMFAC can operate within it to realize multiple control strategies simultaneously. The dynamic linearization parameters of hybrid MG are estimated online to reflect the working condition, and an ET mechanism is designed to reduce the communication burden. The stability of ET-DMFAC is analyzed with the discrete Lyapunov theory and experiments are carried out to verify the effectiveness of the proposed ET-DMFAC strategy under different operating conditions. The outperformance of ET-DMFAC is demonstrated by comparing it with many existing DCS of hybrid AC/DC MG.**

***Index Terms*—Distributed control, event-triggered (ET) control, hybrid microgrid, model-free adaptive control (MFAC).**

NOMENCLATURE

G	Undirected graph of hybrid ac/dc microgrid.
A, D, L	Adjacent matrix, degree matrix, and Laplacian matrix of the graph G.
$\mathcal{N}_{\rm ac}, \mathcal{N}_{\rm dc}$	Total number of ac-DGs and dc-DGs.
$\omega_i, \omega_{\rm ref}$	Angular frequency of ac-DG$_i$ and its reference.
$U_{{\rm ac}i}, U_{\rm acref}$	AC voltage of ac-DG$_i$ and its reference.
δ_i	Phase angle deviation between ac-DG$_i$ and ac bus.
$P_{{\rm ac}i}, P_{{\rm acref}i}$	Active power of ac-DG$_i$ and its reference.
$Q_{{\rm ac}i}, Q_{{\rm acref}i}$	Reactive power of ac-DG$_i$ and its reference.
$n_{{\rm p}i}, n_{{\rm q}i}$	P-f and Q-$U_{\rm ac}$ droop slope of ac-DG$_i$.
$\alpha_{{\rm p}i}, \alpha_{{\rm q}i}$	Frequency and ac voltage restoration coefficient of ac-DG$_i$.
$U_{{\rm dc}j}, U_{\rm dcref}$	DC voltage of dc-DG$_j$ and its reference.
$P_{{\rm dc}j}, P_{{\rm dcref}j}$	Active power of dc-DG$_j$ and its reference.
$n_{{\rm dc}j}$	$P_{\rm dc}$-$U_{\rm dc}$ droop slope of dc-DG$_j$.
$\alpha_{{\rm dc}j}$	DC voltage restoration coefficient of dc-DG$_j$
$P_{\rm ic}, P_{\rm ref}^{\rm ic}$	Active power of interlinking converter (IC) and its reference.
$k_{\rm p}^{\rm IC}, k_{\rm i}^{\rm IC}$	Parameters of DCS's proportional-integral (PI) controller for IC.
$S_{{\rm p}i}, S_{{\rm q}i}$	Active and reactive base power of DG$_i$.
t_m	Time instant for the mth trigger event.
T_s	Sample time of ET-DMFAC.
n_u, n_y	Input and output orders of autoregressive moving average (ARMA) model.
$\phi_{si}, \hat{\phi}_{si}$	Pseudopartial derivative (PPD) of DG$_i$ and its estimated value.
N_i	Set of DGs adjacent to DG$_i$.
η, μ, ρ, σ	Parameters of DMFAC.
θ_{s1}, θ_{s2}	Parameters of ET mechanism.
ω^*, ω_0	Angular frequency of ac bus and its nominal value.
$U_{\rm ac}^*, U_{\rm dc}^*$	Voltage of ac bus and dc bus.
$B_i, G_{{\rm d}i}$	Nominal admittance of ac feeder and dc feeder.

Manuscript received 23 May 2023; revised 25 September 2023; accepted 25 October 2023. Date of publication 21 November 2023; date of current version 13 April 2024. *(Corresponding author: Tao Zheng.)*

Chang Yang, Tao Zheng, Ming Bu, and Pengyu Li are with the Shaanxi Key Laboratory of Smart Grid, School of Electrical Engineering, Xi'an Jiaotong University, Xi'an 710049, China (e-mail: yangchang1996@stu.xjtu.edu.cn; tzheng@mail.xjtu.edu.cn; bm1234@stu.xjtu.edu.cn; lipengyu0628@stu.xjtu.edu.cn).

Josep M. Guerrero is with the Department of Energy Technology, Aalborg University, DK-9220 Aalborg, Denmark (e-mail: joz@energy.aau.dk).

Color versions of one or more figures in this article are available at https://doi.org/10.1109/TIE.2023.3331158.

Digital Object Identifier 10.1109/TIE.2023.3331158

I. INTRODUCTION

IN MODERN power systems, microgrid (MG) not only provides an energy interface to distributed generators (DGs) but also improves the reliability of power supply under extreme conditions [1]. Most DGs output dc power, and converters are required when accessing an ac grid. Thus, energy usage efficiency is undoubtedly reduced. The emergence of the ac/dc MG provides a way to handle this problem. A hybrid ac/dc MG involves several ac-MGs and dc-MGs interconnected through the IC, which controls the power exchange of both sides. The challenge in such a hybrid grid is to design a hierarchical control strategy, which realizes the global power sharing among all DGs as well as frequency and voltage restoration [2], [3].

Despite various hierarchical control strategies have been realized in a single ac-MG [4], [5], [6], [7] or a single dc-MG [8], [9], [10], [11], there still needs further consideration to fulfill

these control objectives simultaneously in the ac/dc MG. In this hybrid structure, ac-DG and dc-DG should cooperate under the assistance of IC, which can be divided into communication-less methods and communication-based methods [12]. As for the communication-less control strategy, complicated controller design is inevitable. In [13], a decentralized power control and management strategy of the ac/dc MG is proposed, but the bus voltage of the ac-MG is only supported by the IC during islanding mode and the voltage may collapse if the IC fails. A dual-droop control [14] and a $P_{dc} - U_{dc}^2$ droop control [15], [16] for the IC are proposed based on local information. However, proportional power dispatch in the hybrid MG is hard to be realized since the power coordination control between ac-DG and dc-DG is ignored. As for the communication-based control strategy, it can be further divided into the centralized control strategy [17], [18], [19] and the distributed control strategy (DCS) [20], [21], [22], [23], [24], [25]. In the centralized framework, a controller collects global information and issues power instructions to the IC and DGs. However, communication between the central controller and DG is required. Controller or communication failure will render a poor control performance of power sharing and even lead to an unstable operation. To deal with the problem of the centralized control strategy, DCS uses a neighbor communication network to mitigate the effect of single-point failure and facilitate the controller design. The challenge is to design a communication-saving controller. In the abovementioned research, the DCS in the hybrid MG is designed with a time-triggered mechanism and the power information should be exchanged among all DGs within a predefined period. In fact, it is not necessary to keep in periodic communication, especially in the steady state [26] and the communication burden can be further reduced if an event-triggered (ET) mechanism is applied. In [27], an ET-based DCS is proposed to improve the economic power dispatch of hybrid MG. However, how to evaluate the impact of ET conditions on the stability of DCS is still an open problem.

The existing implementation of DCS is based on a linear structure and adds a compensation term to the droop control equation. Improper design or changes in working conditions compromise the control performance and cause stability issues [28]. Nowadays, model-free adaptive control (MFAC) attracts much attention due to its simple structure and adaptive regulation ability. Compared with linear structures, MFAC demonstrates greater robustness and adaptability. The dynamic linearization model (DLM) of the control plant is estimated from historical data, which predicts the current working conditions. A variable gain controller can be designed to adapt to the changing conditions accordingly. The existing research is well used in a centralized framework [14], [29], but it is hard to work in a distributed manner without any modification.

To improve the control performance of DCS and reduce the communication burden, this article proposes a distributed model-free adaptive control (DMFAC) strategy with ET mechanism (ET-DMFAC) for global power sharing and voltage/frequency restoration in a hybrid ac/dc MG. The main contributions can be summarized as follows.

1) A unified control framework of the hybrid ac/dc MG is developed. This framework can represent three types of droop control among different DGs in a unified form. In contrast to the traditional DCSs in the hybrid MG [20], [21], which specifically define each controller under different droop controls, the unified control framework uses only one set of control equations to express the DCS, simplifying the design process.
2) A novel DCS called ET-DMFAC is proposed to achieve global power sharing among all the DGs and voltage/frequency restoration in the hybrid MG simultaneously. The proposed approach utilizes historical sampling data to estimate the current state of DGs and realizes the control objectives in a distributed manner. Compared with the model-based strategy [25], complex modeling of the MG can be avoided. Furthermore, it is adaptive to different working conditions, such as the change of the droop slope, in which degraded control performance may occur under the PI-based DCS [20], [21].
3) An ET mechanism is designed to reduce the communication burden. Compared with the continuous communication mode adopted [20], [21], [22], [23], [24], [25], the ET mechanism can determine the time instant for information update. This mechanism is based on the local information, enabling the prevention of unnecessary connections during the intervals between two trigger events.
4) The stability of the proposed control strategy is analyzed by using the discrete Lyapunov theory. The parameters of the ET condition can be designed based on the analysis.
5) To verify the effectiveness of the proposed control strategy, a laboratory ac/dc MG is developed with real converters. With this setup, the proposed approach is tested in different operation conditions. Comprehensive comparisons are conducted between the proposed method and the state-of-the-art methods.

The rest of this article is organized as follows. The control objectives of the DCS in the hybrid ac/dc MG are developed in Section II, and the proposed ET-DMFAC strategy with stability analysis is presented in Section III. In Section IV, experiments are carried out to validate the performance of the proposed control strategy under various operating conditions. Finally, Section V concludes this article.

II. Control Objectives of DCS

A. System Architecture

A hybrid ac/dc MG consists of ac-MG and dc-MG that are interconnected through an IC. The representative topology of a hybrid ac/dc MG is shown in Fig. 1 [21], [24]. The ac-DG and dc-DG are connected to the ac bus and dc bus through feeders, while the IC connects the two subgrids, acting as a bridge to transfer active power between them. Some local information, such as output power, frequency, and voltage, are exchanged between the neighbor DGs through a distributed communication network. As shown in Fig. 1, the local communication links within a single MG are illustrated in red dashed lines, the intercommunication links between ac-MG and dc-MG are illustrated in blue dashed lines, and the communication involving the IC is illustrated in green dashed lines.

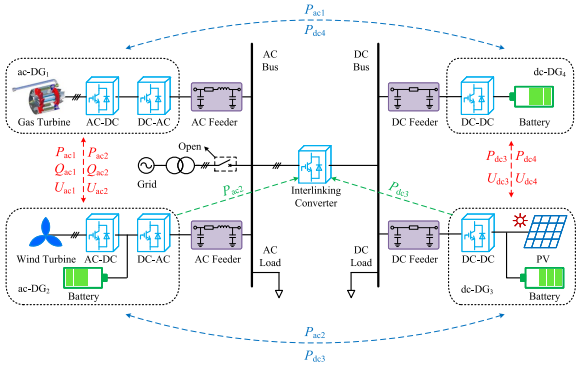

Fig. 1. Hybrid AC/DC MG with distributed communication network.

Generally speaking, in a hybrid ac/dc MG, the ac-DG adopts P-f and Q-$U_{\rm ac}$ droop control and the dc-DG adopts $P_{\rm dc}$-$U_{\rm dc}$ droop control, which can be expressed as in the following. For notional convenience, the ac-DGs are indexed from 1 to $\mathcal{N}_{\rm ac}$, whereas the dc-DGs are indexed from $\mathcal{N}_{\rm ac}+1$ to $\mathcal{N}_{\rm ac}+\mathcal{N}_{\rm dc}$

$$\begin{cases} \omega_i = \omega_{\rm ref} - n_{{\rm p}i}(P_{{\rm ac}i} - P_{{\rm acref}i}) \\ U_{{\rm ac}i} = U_{\rm acref} - n_{{\rm q}i}(Q_{{\rm ac}i} - Q_{{\rm acref}i}) \\ U_{{\rm dc}j} = U_{\rm dcref} - n_{{\rm dc}j}(P_{{\rm dc}j} - P_{{\rm dcref}j}) \\ i = 1, 2, \ldots, \mathcal{N}_{\rm ac} \\ j = \mathcal{N}_{\rm ac}+1, \mathcal{N}_{\rm ac}+2, \ldots, \mathcal{N}_{\rm ac}+\mathcal{N}_{\rm dc}. \end{cases} \tag{1}$$

B. Communication Network

The distributed communication network (excluding the links between DG and IC) can be represented as an undirected graph $G = (\mathbb{V}, \mathbb{E}, A)$, where $\mathbb{V} = 1, 2, \ldots, \mathcal{N}_{\rm ac}+\mathcal{N}_{\rm dc}$ is the set of vertices, $\mathbb{E} \subset \mathbb{V} \times \mathbb{V}$ is the set of edges, and A is the adjacency matrix. If the edge $(i, j) \in \mathbb{E}$, then $a_{ij} = 1$, otherwise $a_{ij} = 0$. The degree of vertice i can be defined as $d_i = \sum_{j=1, j\neq i}^{\mathcal{N}_{\rm ac}+\mathcal{N}_{\rm dc}} a_{ij}$ and the degree matrix can be expressed as $D = {\rm diag}_i(d_i)$. The Laplacian matrix $L = D - A$ is symmetric.

C. Control Objectives

In the hybrid ac/dc MG, DCS is responsible for two control objectives: power sharing among all the DGs and voltage/frequency restoration. These objectives can be realized by adjusting the reference of DG's output power $P_{\rm acref}$, $Q_{\rm acref}$, and $P_{\rm dcref}$ dynamically with the help of the distributed communication network.

1) *Power Sharing:* Regarding the active control, ac-DGs and dc-DGs should share the active power according to a specified proportion. Particularly, in the dc-MG, it is challenging to share the active power relying solely on the $P_{\rm dc}$-$U_{\rm dc}$ droop control. The different impedances of the dc feeders deviate the DG's output and compensation is necessary. Similarly, regarding the reactive power, the same problem occurs in the reactive power sharing among ac-DGs. Therefore, the control objectives of power sharing in the hybrid ac/dc MG can be expressed as

$$\begin{cases} P_i^* = P_j^* & \forall i, j \in [1, \mathcal{N}_{\rm ac}+\mathcal{N}_{\rm dc}] \\ Q_i^* = Q_j^* & \forall i, j \in [1, \mathcal{N}_{\rm ac}] \end{cases} \tag{2}$$

where $P_i^* = P_i/S_{{\rm p}i}$ and $Q_i^* = Q_i/S_{{\rm q}i}$ are the unit values of the active power and reactive power. It should be noted that the power can be evenly shared or proportionally shared among DGs. In (2), the unit value of output power among all DGs reaches a consensus and the portion of the output power depends on the amount of $S_{{\rm p}i}$ and $S_{{\rm q}i}$.

2) *Voltage and Frequency Restoration:* According to (1), the frequency, ac voltage, and dc voltage of ${\rm DG}_i$ deviate from their reference due to droop control. The second goal of the DCS is to restore the voltage and frequency. The control objectives of ac-DG and dc-DG can be described as

$$\begin{cases} \omega_{\rm ref} = \omega_i, \forall i \in [1, \mathcal{N}_{\rm ac}] \\ U_{\rm acref} = \dfrac{1}{\mathcal{N}_{\rm ac}} \sum_{i=1}^{\mathcal{N}_{\rm ac}} U_{{\rm ac}i} \end{cases} \tag{3}$$

$$U_{\rm dcref} = \frac{1}{\mathcal{N}_{\rm dc}} \sum_{i=\mathcal{N}_{\rm ac}+1}^{\mathcal{N}_{\rm ac}+\mathcal{N}_{\rm dc}} U_{{\rm dc}i}. \tag{4}$$

III. ET-DMFAC Strategy

To realize the control objectives and improve the control performance, an ET-DMFAC is proposed in this section. A traditional MFAC [14] is redesigned in a distributed manner. Herein, model-free calls for the controller to break away from the complex modeling of MG. Two universal models, the ARMA model and the DLM, are utilized to formulate the hybrid MG. Besides, an ET mechanism is used to reduce the communication burden. The stability of ET-DMFAC is analyzed with the Lyapunov theory.

A. Overview

The control diagram of an ET-DMFAC is shown in Fig. 2, including the control of ac-DG, dc-DG, and IC connected through a communication network. For the ac-DG and dc-DG, a time-varying parameter of DLM called PPD is estimated (see Section III-C). Based on it, the DMFAC calculates the power reference of the droop control by combining the information from the neighbor DGs. The setting value of voltage and frequency calculated by the droop control will be sent to the dual loop control for PWM signal generation. The ET mechanism controls the interval of power information exchange between the neighbors. With ET-DMFAC, ac-DGs and dc-DGs tend to share the output power with each other and the control objectives are to achieve a consensus among all the DGs.

However, the imbalance load between the ac-MG and the dc-MG presents an obstacle to effective power sharing. The role of IC is to balance the active load between both subgrids. It should be noted that communication between ac-DG and dc-DG should be limited, as multiple DGs accessing the MG can potentially impose a significant communication burden. Herein, two unidirectional communication links, one from an ac-DG and the other from a dc-DG, are established as illustrated in Fig. 2. The control equation of IC can be expressed in the following equation. The IC obtains the power information uploaded separately from the ac-DG and the dc-DG, and then, minimizes the difference in order to achieve a load balance. When the

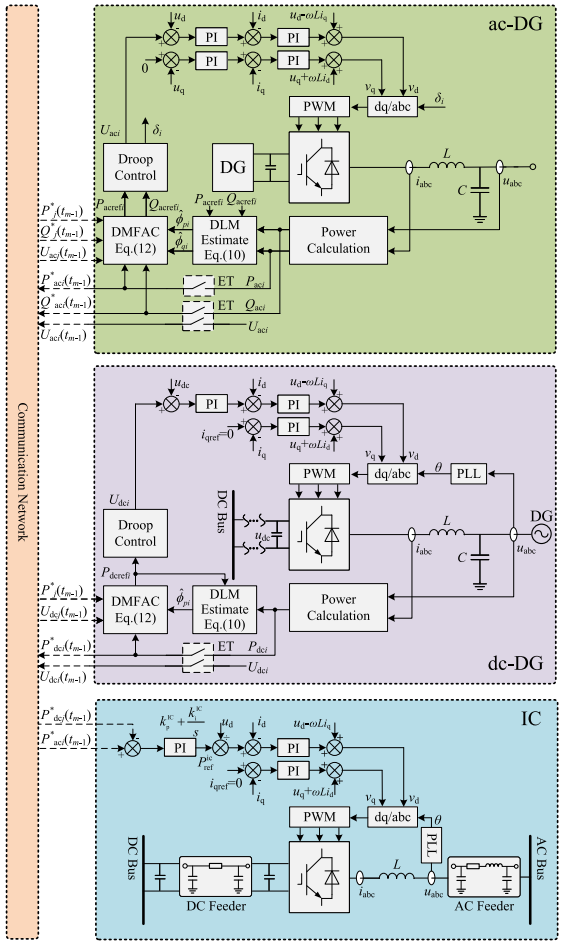

Fig. 2. Control diagram of an ET-DMFAC.

normalized active power of the ac-DG exceeds that of the dc-DG, it indicates that the ac-MG has a higher load demand than the dc-MG. In this case, the IC should deliver power to the ac-MG. Otherwise, the IC should deliver power to the dc-MG

$$\begin{cases} P_{\text{ref}}^{\text{ic}} = \left(k_{\text{p}}^{\text{IC}} + \dfrac{k_{\text{i}}^{\text{IC}}}{s}\right)\left(P_{\text{ac}i}^{*}(t_{m-1}) - P_{\text{dc}j}^{*}(t_{m-1})\right) \\ i \in [1, \mathcal{N}_{\text{ac}}], j \in [\mathcal{N}_{\text{ac}}+1, \mathcal{N}_{\text{ac}}+\mathcal{N}_{\text{dc}}]. \end{cases} \tag{5}$$

B. Unified Control Framework

Within the hybrid ac/dc MG, three types of droop control are employed, which increase the complexity of the DCS. To facilitate the controller design, a unified control framework is established and the droop control equation in (1) can be expressed in a unified and discrete form as

$$x_{si}(k) = x_{s\text{ref}} - n_{si}(y_{si}(k) - u_{si}(k-1)), i \in [1, \mathcal{N}_{\text{ac}} + \mathcal{N}_{\text{dc}}] \tag{6}$$

where $s \in \{\text{p}, \text{q}, \text{dc}\}$ indicates different types of droop control. The corresponding variables of droop control in the unified framework are given in Table I.

TABLE I
CONTROL VARIABLES IN THE UNIFIED FRAMEWORK

Framework	Active control		Reactive control
	P-f droop ($s=\text{p}$)	P_{dc}-U_{dc} droop ($s=\text{dc}$)	Q-U_{ac} droop ($s=\text{q}$)
u_{si}	$P_{\text{acref}i}^{*}$	$P_{\text{dcref}i}^{*}$	$Q_{\text{acref}i}^{*}$
y_{si}	$P_{\text{ac}i}^{*}$	$P_{\text{dc}i}^{*}$	$Q_{\text{ac}i}^{*}$
n_{si}	$S_{\text{p}i}n_{\text{p}i}$	$S_{\text{p}i}n_{\text{dc}i}$	$S_{\text{q}i}n_{\text{q}i}$
x_{si}	ω_i	$U_{\text{dc}i}$	$U_{\text{ac}i}$
$x_{s\text{ref}}$	ω_{ref}	U_{dcref}	U_{acref}

For convenience, the ET-DMFAC is described according to the $(m-1)$th and the mth trigger event without loss of generality, i.e., $t \in [t_{m-1}, t_m)$. $u_{si}(k)$ and $y_{si}(k)$ are defined at the instant $t = t_{m-1} + kT_s$.

C. Dynamic Linearization Model of DG

The droop-controlled DG in a hybrid ac/dc MG can be regarded as a single-control plant. The power reference u_{si} and the output power y_{si} denote the input and output variable, respectively. Their relationship can be depicted by using an ARMA model [14], which can be expressed as

$$y(k+1) = f(y(k), \ldots, y(k-n_y), u(k), \ldots, u(k-n_u)). \tag{7}$$

In (7), n_y and n_u are unknown positive integers, which vary with the scale of the hybrid MG. The ARMA model can be linearized as (8) if the following two assumptions are satisfied [14], [30].

Assumption 1: The function $f(\cdot)$ has continuous partial derivatives with respect to $u(k), u(k-1), \ldots, u(k-n_u)$.

Assumption 2: The control system in (7) is generalized Lipschitz, that is to say $\forall k \in \mathbb{N}^{+}$, $|\Delta y(k+1)| \le b|\Delta u(k)|$ $\forall |\Delta u(k)| \ne 0$

$$y_{si}(k+1) - y_{si}(k) = \phi_{si}(k)(u_{si}(k) - u_{si}(k-1)). \tag{8}$$

It is hard to acquire the PPD directly due to its time-varying feature. Thus, an optimization objective is built taking into account the historical data [31], [32], which can be depicted as (9) and solved by using the gradient descent algorithm shown in (10)

$$\begin{aligned} \min J(\hat{\phi}_{si}(k)) &= (\Delta y_{si}(k+1) - \hat{\phi}_{si}(k)\Delta u_{si}(k))^2 \\ &\quad + \mu(\hat{\phi}_{si}(k) - \hat{\phi}_{si}(k-1))^2 \end{aligned} \tag{9}$$

$$\begin{aligned} \hat{\phi}_{si}(k) &= \hat{\phi}_{si}(k-1) + \frac{\eta \Delta u_{si}(k-1)}{\mu + \Delta u_{si}(k-1)^2} \\ &\quad \times (\Delta y_{si}(k) - \hat{\phi}_{si}(k-1)\Delta u_{si}(k-1)) \end{aligned} \tag{10}$$

where $\Delta y_{si}(k+1) = y_{si}(k+1) - y_{si}(k)$ and $\Delta u_{si}(k) = u_{si}(k) - u_{si}(k-1)$. $\eta \in (0,1)$ and $\mu > 0$ are two parameters for DLM estimate.

D. ET-DMFAC

To achieve the control objectives described in (2)–(4), the power reference is updated by using the DLM of DG. It can be transformed into another optimization problem expressed as

$$\begin{cases} \min J(u_{si}(k)) = \psi_{si}^2(k) + \sigma(u_{si}(k) - u_{si}(k-1))^2 \\ \psi_{si}(k) = \alpha_{si}(x_{\text{sref}} - \overline{x}_s(k)) + \sum_{j\in N_i} a_{ij}(y_{sj}(t_{m-1}) \\ \qquad -y_{si}(t_{m-1})) \end{cases} \tag{11}$$

where $\overline{x}_s(k) = (x_{si}(k) + \sum_{j\in N_i} x_{sj}(t_{m-1}))/(1+d_i)$ is the average value of x_s considering DG_i and its neighbor DGs.

In (11), $\psi_{si}(k)$ contains two terms that correspond to the two control objectives. $\psi_{si}(k) = 0$ means that control objectives can be satisfied simultaneously. In other words, both power sharing and voltage/frequency restoration can be realized. The solution of (11) can be obtained by

$$u_{si}(k) = u_{si}(k-1) + \frac{\rho d_i \hat{\phi}_{si}(k)}{\sigma + |d_i \hat{\phi}_{si}(k)|^2} \psi_{si}(k) \tag{12}$$

where $\rho \in (0,1)$ and $\sigma > 0$ are two parameters for DMFAC.

According to (12), the control gain $\gamma_{si}(k) = (\rho d_i \hat{\phi}_{si}(k))/(\sigma + |d_i \hat{\phi}_{si}(k)|^2)$ changes with the dynamic of the linearized model during power reference update. The parameter of DLM $\hat{\phi}_{si}(k)$ is estimated online. It should be noted that $\hat{\phi}_{si}(k)$ takes into account the current working condition. Therefore, DMFAC is adaptive to various working conditions and maintains a good original performance when some parameters of the primary control change, e.g., the droop slope.

Instead of the time-triggered DCS, which requires some redundant communication, in this article, an ET mechanism is designed. Define $\epsilon_{si}(k) = y_{si}(k) - y_{si}(t_{m-1})$ and $\zeta_{si}(k) = x_{si}(k) - x_{si}(t_{m-1})$, and the trigger condition of DG_i is denoted as

$$g_i(\epsilon_{si}, \zeta_{si}, \psi_{si}) = \theta_{s1} \|\epsilon_{si}(k)\|^2 + \theta_{s2} \|\zeta_{si}(k)\|^2 - \|\psi_{si}(k)\|^2 \geq 0. \tag{13}$$

Equation (13) contains two update errors, $\epsilon_{si}(k)$ and $\zeta_{si}(k)$, and one control error $\psi_{si}(k)$. $\epsilon_{si}(k)$ represents the difference of DG_i's output power between the current time $t = t_{m-1} + kT_s$ and the previously triggered instant $t = t_{m-1}$. Large $\|\epsilon_{si}(k)\|$ indicates a significant difference between the DG_i's actual output power and the power information perceived by other DGs. Consequently, an update of DG_i's power information becomes necessary. A similar analysis can be conducted with the update error $\zeta_{si}(k)$. Regarding the control error $\psi_{si}(k)$, if $\|\psi_{si}(k)\|$ is excessive, it indicates that the ET-DMFAC has not reached the steady state. The update error is caused by the transient process and the frequent information update is not necessary. However, the reduction of communication may deteriorate the control performance and it is necessary to compromise among these errors by considering the parameters θ_{s1} and θ_{s2}.

It should be noted that the trigger condition of DG_i is only related to the variables of itself and irrelevant to other DGs. Therefore, before the trigger condition is satisfied, DG_i does not need to acquire the power information of other DGs. When the trigger condition is met, only related power information is updated. For example, if the condition of active control is satisfied in DG_i, the active power should be sent to its neighbors regardless of the reactive power information.

E. Stability Analysis

Herein, the discrete Lyapunov theory is employed to verify the stability of ET-DMFAC. First, an assumption and some lemmas are introduced. Detailed proof of these lemmas can be found in the Appendix.

Assumption 3: The output power of IC can track its reference without any error, that is to say, $P_{\text{ref}}^{\text{ic}}(k) = P_{\text{ic}}(k)$.

Lemma 1: If the symmetric matrix $M \in \mathbb{R}^{N\times N}$ is a substochastic matrix, then the matrix $I - M^T M$ is positive definite and its eigenvalues satisfy $\lambda(I - M^T M) > 0$.

Lemma 2: For the symmetric matrix $M \in \mathbb{R}^{N\times N}$, $\lambda_{\min}$ is the minimum eigenvalue, then $\forall x \in \mathbb{R}^N$, $\lambda_{\min} x^T x \leq x^T M x$.

To analyze the stability of ET-DMFAC, a simplified model of MG is established. The discrete-time model of ac-DG, dc-DG, and IC can be expressed by (14)–(16), respectively [33]

$$\begin{cases} \omega_i(k+1) = \omega_i(k) - n_{\text{p}i}\Delta P_{\text{ac}i}(k+1) + n_{\text{p}i}\Delta P_{\text{acref}i}(k) \\ U_{\text{ac}i}(k+1) = U_{\text{ac}i}(k) - n_{\text{q}i}\Delta Q_{\text{ac}i}(k+1) + n_{\text{q}i}\Delta Q_{\text{acref}i}(k) \\ \delta_i(k+1) = \delta_i(k) + T_s(\omega_i(k+1) - \omega^*(k)) \\ P_{\text{ac}i}(k+1) = P_{\text{ac}i}(k) + \Delta U_{\text{ac}i}(k+1) B_i U_{\text{ac}}^*(k) \sin(\delta_i(k)) \\ \qquad + (\delta_i(k+1) - \delta_i(k)) B_i U_{\text{ac}i}(k) U_{\text{ac}}^*(k) \cos(\delta_i(k)) \\ Q_{\text{ac}i}(k+1) = Q_{\text{ac}i}(k) + \Delta U_{\text{ac}i}(k+1) B_i (2U_{\text{ac}i}(k) \\ \qquad - U_{\text{ac}}^*(k)\cos(\delta_i(k))) + (\delta_i(k+1) \\ \qquad - \delta_i(k)) B_i U_{\text{ac}i}(k) U_{\text{ac}}^*(k) \sin(\delta_i(k)) \end{cases} \tag{14}$$

$$\begin{cases} U_{\text{dc}i}(k+1) = U_{\text{dc}i}(k) - n_{\text{dc}i}\Delta P_{\text{dc}i}(k+1) + n_{\text{dc}i}\Delta P_{\text{dcref}i}(k) \\ P_{\text{dc}i}(k+1) = P_{\text{dc}i}(k) + \Delta U_{\text{dc}i}(k+1) G_{\text{d}i} U_{\text{dc}}^*(k) \end{cases} \tag{15}$$

$$\begin{cases} \sum_{i=1}^{\mathcal{N}_{\text{ac}}} S_{\text{p}i} y_{\text{p}i}(k) + P_{\text{ic}}(k) = P_L^{\text{ac}} \\ \sum_{i=\mathcal{N}_{\text{ac}}+1}^{\mathcal{N}_{\text{ac}}+\mathcal{N}_{\text{dc}}} S_{\text{p}i} y_{\text{dc}i}(k) - P_{\text{ic}}(k) = P_L^{\text{dc}} \end{cases} \tag{16}$$

where $B_i = 1/(\omega_0 L_i)$ is the nominal admittance of the ac feeder and $G_{\text{d}i} = 1/R_{\text{d}i}$ is the nominal admittance of the dc feeder.

Considering that the frequency of ac-DG ω_i and the frequency of ac bus ω^* are approximately equal, it can be observed that the phase angle deviation δ_i approaches 0. Consequently, the approximations $\sin(\delta_i) \approx 0$ and $\cos(\delta_i) \approx 1$ can be made. Therefore, the dynamic linearization parameter $\phi_{si}(k)$ of ac-DG and dc-DG can be obtained as (17) under the system models (14) and (15)

$$\begin{cases} \phi_{\text{p}i}(k) = \dfrac{n_{\text{p}i} S_{\text{p}i} T_s B_i U_{\text{ac}i}(k) U_{\text{ac}}^*(k)}{1 + n_{\text{p}i} S_{\text{p}i} T_s B_i U_{\text{ac}i}(k) U_{\text{ac}}^*(k)} \\ \phi_{\text{q}i}(k) = \dfrac{n_{\text{q}i} S_{\text{q}i} B_i (2U_{\text{ac}i}(k) - U_{\text{ac}}^*(k))}{1 + n_{\text{q}i} S_{\text{q}i} B_i (2U_{\text{ac}i}(k) - U_{\text{ac}}^*(k))} \\ \phi_{\text{dc}i}(k) = \dfrac{n_{\text{dc}i} S_{\text{p}i} G_{\text{d}i} U_{\text{dc}}^*(k)}{1 + n_{\text{dc}i} S_{\text{p}i} G_{\text{d}i} U_{\text{dc}}^*(k)}. \end{cases} \tag{17}$$

Consequently, (8) can represent the model of DGs described in (14) and (15), which can be expressed in the vector form as

$$\vec{y}_s(k+1) = \vec{y}_s(k) + \Phi_s(k)(\vec{u}_s(k) - \vec{u}_s(k-1)) \tag{18}$$

where $\Phi_s(k) = \text{diag}_i(\phi_{si}(k))$.

Equations (6) and (12) can also be expressed in the vector form as

$$\begin{cases}\vec{x}_{si}(k)=\vec{x}_{\text{sref}}-N_s(\vec{y}_s(k)-\vec{u}_s(k-1))\\ \vec{u}_s(k)=\vec{u}_s(k-1)+\Gamma_s(k)\vec{\psi}_s(k)\end{cases} \tag{19}$$

where $N_s=\text{diag}_i(n_{si})$ and $\Gamma_s(k)=\text{diag}_i((\rho d_i\hat{\phi}_{si}(k))/(\sigma+|d_i\hat{\phi}_{si}(k)|^2))$.

The ET-DMFAC in (11) can be expressed as

$$\begin{aligned}\vec{\psi}_s(k)=&(\Lambda_sN_s(I+A)-L)\vec{y}_s(k)-\Lambda_sN_s(I+A)\vec{u}_s(k-1)\\&+L\vec{\epsilon}_s(k)+\Lambda_sA\vec{\zeta}_s(k)\end{aligned} \tag{20}$$

where $\Lambda_s=\text{diag}_i(\alpha_{si}/(1+d_i))$.

According to (18) and (19), (20) can be transformed into

$$\begin{aligned}&\vec{\psi}_s(k+1)-L\vec{\epsilon}_s(k+1)-\Lambda_sA\vec{\zeta}_s(k+1)\\&=(\underbrace{I-L\Phi_s(k)\Gamma_s(k)}_{M_{s1}(k)}-\underbrace{\Lambda_sN_s(I+A)(I-\Phi_s(k))\Gamma_s(k)}_{M_{s2}(k)})\vec{\psi}_s(k)\\&\quad-L\vec{\epsilon}_s(k)-\Lambda_sA\vec{\zeta}_s(k)\\&=M_s(k)\vec{\psi}_s(k)-L\vec{\epsilon}_s(k)-\Lambda_sA\vec{\zeta}_s(k).\end{aligned} \tag{21}$$

According to *Assumption 2*, the inequality (22) holds if the parameter σ is selected as $\sigma>\sigma_{\min}>b^2>0$. Therefore, by selecting the appropriate value of ρ, it ensures that $M_{s1}(k)$ is a double stochastic matrix and $M_{s2}(k)$ is a nonnegative matrix. The restoration coefficient α_{si} can be selected to guarantee that $M_s(k)$ is a substochastic matrix

$$\frac{d_i\phi_{si}(k)\hat{\phi}_{si}(k)}{\sigma+|d_i\hat{\phi}_{si}(k)|^2}<\frac{d_i\hat{\phi}_{si}(k)}{2\sqrt{\sigma}d_i\hat{\phi}_{si}(k)}b<\frac{b}{2\sqrt{\sigma}}<\frac{1}{2}. \tag{22}$$

Regarding the IC, (23) can be obtained according to (16)

$$\begin{cases}P_{\text{ic}}(k+1)=P_{\text{ic}}(k)-\sum_{i=1}^{\mathcal{N}_{\text{ac}}}S_{\text{p}i}(y_{\text{p}i}(k+1)-y_{\text{p}i}(k))\\ P_{\text{ic}}(k+1)=P_{\text{ic}}(k)+\sum_{i=\mathcal{N}_{\text{ac}}+1}^{\mathcal{N}_{\text{ac}}+\mathcal{N}_{\text{dc}}}S_{\text{p}i}(y_{\text{dc}i}(k+1)-y_{\text{dc}i}(k)).\end{cases} \tag{23}$$

Herein, a Lyapunov function is selected as $V(k)=V_1(k)+V_2(k)$, which contains two terms, depicted as

$$\begin{cases}V_1(k)=(\vec{\psi}_s(k)-L\vec{\epsilon}_s(k)-\Lambda_sA\vec{\zeta}_s(k))^T(\vec{\psi}_s(k)-L\vec{\epsilon}_s(k)\\ \qquad -\Lambda_sA\vec{\zeta}_s(k))\\ V_2(k)=(\beta_{\text{ac}}\sum_{i=1}^{\mathcal{N}_{\text{ac}}}S_{\text{p}i}y_{\text{p}i}(k)-\beta_{\text{dc}}\sum_{i=\mathcal{N}_{\text{ac}}+1}^{\mathcal{N}_{\text{ac}}+\mathcal{N}_{\text{dc}}}S_{\text{p}i}y_{\text{dc}i}(k))^2\end{cases} \tag{24}$$

where $\beta_{\text{ac}}=1/\sum_{i=1}^{\mathcal{N}_{\text{ac}}}S_{\text{p}i}$ and $\beta_{\text{dc}}=1/\sum_{i=\mathcal{N}_{\text{ac}}+1}^{\mathcal{N}_{\text{ac}}+\mathcal{N}_{\text{dc}}}S_{\text{p}i}$.

For the first term, (25) can be obtained according to (21)

$$\begin{aligned}&\Delta V_1(k+1)=V_1(k+1)-V_1(k)\\&=-\vec{\psi}_s^T(k)(I-M_s^T(k)M_s(k))\vec{\psi}_s(k)+\\&\quad2\vec{\psi}_s^T(k)(I-M_s(k))L\vec{\epsilon}_s(k)+2\vec{\psi}_s^T(k)(I-M_s(k))\Lambda_sA\vec{\zeta}_s(k).\end{aligned} \tag{25}$$

Define $R_s(k)=I-M_s^T(k)M_s(k)$. Following *Lemma 1*, the minimum eigenvalue of $R_s(k)$ $\lambda_{\min}^R>0$. Considering the inequality $x^Ty\le\frac{\kappa}{2}x^Tx+\frac{2}{\kappa}y^Ty,\kappa>0$ and selecting $\kappa=\lambda_{\min}^R/4$, (25) can be upper bounded as follows:

$$\begin{aligned}&\Delta V_1(k+1)\le-\lambda_{\min}^R\left\|\vec{\psi}_s(k)\right\|^2\\&+\frac{\lambda_{\min}^R}{4}\left\|\vec{\psi}_s(k)\right\|^2+\frac{16}{\lambda_{\min}^R}\|I-M_s(k)\|^2\|L\|^2\|\vec{\epsilon}_s(k)\|^2\\&+\frac{\lambda_{\min}^R}{4}\left\|\vec{\psi}_s(k)\right\|^2+\frac{16}{\lambda_{\min}^R}\|I-M_s(k)\|^2\|\Lambda_s\|^2\|A\|^2\left\|\vec{\zeta}_s(k)\right\|^2\\&=-\frac{\lambda_{\min}^R}{2}\left\|\vec{\psi}_s(k)\right\|^2+\frac{16}{\lambda_{\min}^R}\|I-M_s(k)\|^2\|L\|^2\|\vec{\epsilon}_s(k)\|^2\\&+\frac{16}{\lambda_{\min}^R}\|I-M_s(k)\|^2\|\Lambda_s\|^2\|A\|^2\left\|\vec{\zeta}_s(k)\right\|^2.\end{aligned} \tag{26}$$

According to the ET condition, the parameters θ_{s1} and θ_{s2} can be selected as

$$\begin{aligned}\theta_{s1}&=\frac{32}{\xi_1(\lambda_{\min}^R)^2}\|I-M_s(k)\|^2\|L\|^2\\\theta_{s2}&=\frac{32}{\xi_2(\lambda_{\min}^R)^2}\|I-M_s(k)\|^2\|\Lambda_s\|^2\|A\|^2\end{aligned}$$

where $\xi_1,\xi_2\in(0,1)$ are scale factors.

Then, the inequality in (27) can be obtained as follows:

$$\begin{aligned}\Delta V_1(k+1)<&\frac{\lambda_{\min}^R}{2}\left(\xi_1\theta_{s1}\|\vec{\epsilon}_s(k)\|^2+\xi_2\theta_{s2}\|\vec{\zeta}_s(k)\|^2\right.\\&\left.-\|\vec{\psi}_s(k)\|^2\right)\\<&\frac{\lambda_{\min}^R}{2}\left(\theta_{s1}\|\vec{\epsilon}_s(k)\|^2+\theta_{s2}\|\vec{\zeta}_s(k)\|^2-\|\vec{\psi}_s(k)\|^2\right).\end{aligned} \tag{27}$$

Considering the trigger condition in (13), $\Delta V_1(k+1)<0$ is reasonable. The above analysis ensures power sharing within a single MG. It is important to observe that any imbalance load between the ac-MG and the dc-MG leads to a deviation of power distribution in the ac-DG and dc-DG. Consequently, the IC is involved in maintaining load balancing.

As for the second term of the Lyapunov function, by combining (5), (23), and *Assumption 3*, (28) can be obtained if the power sharing of a single MG is achieved and a small value of k_{p}^{IC} is selected

$$\Delta V_2(k+1)=-\frac{2(\beta_{\text{ac}}+\beta_{\text{dc}})}{k_{\text{i}}^{\text{IC}}T_s}(P_{\text{ic}}(k+1)-P_{\text{ic}}(k))^2<0. \tag{28}$$

Therefore, $\Delta V(k+1)=\Delta V_1(k+1)+\Delta V_2(k+1)<0$ holds, and the proposed DCS is asymptotically stable.

Remark: The selection of ξ_1 and ξ_2 is a tradeoff between communication burden and control performance. If ξ_1 and ξ_2 approach 1, the communication cost can be reduced to a lower level. However, the control objectives may be achieved with a long transient process although the stability can be guaranteed. On the other hand, if ξ_1 and ξ_2 approach 0, the trigger condition will change from ET to time triggered. The best control

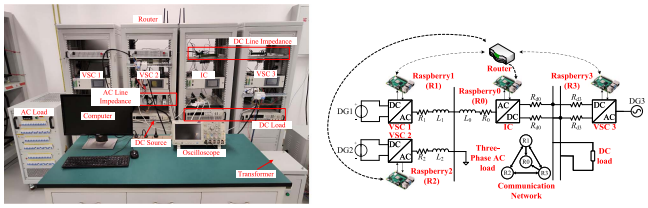

(a) (b)

Fig. 3. Experiment platform of the hybrid MG. (a) Instruments. (b) Grid overview.

TABLE II
SYSTEM PARAMETERS OF THE HYBRID MG IN EXPERIMENTS

Classification	Parameters	Value
VSC	AC rms voltage	173V
	Frequency	50Hz
	DC voltage	300V
	Filter inductance	1.2 mH
	Filter capacitor	16 μF
AC-MG	R_0, L_0	0.4 Ω, 0.33 mH
	R_1, L_1	1.1 Ω, 2.67 mH
	R_2, L_2	0.7 Ω, 1.45 mH
	AC Load	900+500j VA
DC-MG	R_{d0}	0.5 Ω
	R_{d1}	1 Ω
	DC Load	600 W

performance can be achieved but the communication burden is heaviest.

IV. EXPERIMENTAL RESULTS

A. Experiment Setup

To verify the feasibility of the proposed control strategy, a hybrid ac/dc MG experiment platform is established in the laboratory, which is shown in Fig. 3(a). The topology of this ac/dc MG is depicted in Fig. 3(b) and it primarily consists of four two-level voltage source converters (VSC). The parameters of VSC and line impedance are detailed in Table II. VSC1 and VSC2 serve as two ac-DGs, while VSC3 serves as a dc-DG. There are 900+500jVA ac base load and 600 W dc base load in the experiment. The primary control algorithm and ET-DMFAC strategy are implemented through the TMS320F28335 DSP controller configured in the VSC and the Raspberry Pi controller, respectively. The two controllers are connected through a high-speed CAN serial bus, which guarantees the bandwidth between DMFAC and the primary control. All of the control parameters are listed in Table III.

B. Control Performance

The experiment is manipulated in three stages.

1) At $t = 10$ s, put the proposed ET-DMFAC into operation.
2) At $t = 30$ s, increase 300 var reactive load in the ac-MG.
3) At $t = 50$ s, decrease 300 W active load in the dc-MG.

TABLE III
CONTROL PARAMETERS OF THE HYBRID MG IN EXPERIMENTS

Classification	Parameters	value
VSC1 and VSC2	n_p	0.05Hz/kW
	n_q	20V/kvar
	α_p	1kW/Hz
	α_q	0.01 kvar/V
	η, μ, ρ, σ	0.005, 0.02, 0.005, 0.02
	θ_{p1}, θ_{p2}	4, 9
	θ_{q1}, θ_{q2}	0.4, 0.9
VSC3	n_{dc}	30V/kW
	α_{dc}	0.01kW/V
	η, μ, ρ, σ	0.005, 0.02, 0.005, 0.02
	$\theta_{dc1}, \theta_{dc2}$	0.4, 0.9
IC	k_p^{IC}, k_i^{IC}	0.01, 10

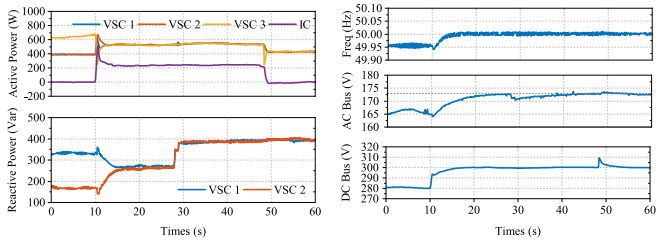

(a) (b)

Fig. 4. Experiment results under the step change of AC and DC load. (a) Active power and reactive power. (b) Frequency, AC bus voltage, and DC bus voltage.

The results are shown in Fig. 4, which illustrate the active and reactive power of the DG, the frequency, and ac bus voltage as well as the dc bus voltage. After applying ET-DMFAC, power sharing among all the DGs is realized. The frequency and voltage return to their nominal value. There are two drops of VSC3's active power. The first one corresponds to the transient process, while the second one originates from the load change in dc-MG. It should be noted that the large overshoot can be suppressed by adjusting the control parameters but resulting in a slow transient process.

The ET-DMFAC can also achieve any proportion of power sharing, e.g., P_1:P_2:P_3 = 3:2:1 and Q_1:Q_2 = 1:1. In this approach, the power information obtained from the adjacent DG are normalized, that is to say, $y_{si}^* = y_{si}/S_{si}$. The normalized power can achieve a consensus, subsequently enabling the share of output power according to the ratio of S_{si}. Herein, the ratio of S_{si} satisfies S_{p1}:S_{p2}:S_{p3} = 3:2:1 and S_{q1}:S_{q2} = 1:1. The result of proportional power sharing is shown in Fig. 5(a), which demonstrates that the ET-DMFAC ensures an accurate ratio of output power sharing among different VSCs.

C. Plug and Play

In ET-DMFAC, DG that does not communicate with the IC has the capability of plug and play. Herein, an experiment is conducted to illustrate the plug-and-play process of VSC2. In Fig. 5(b), VSC2 switches OFF at $t = 10$ s, resulting in the load of

TABLE IV
COMPARISONS WITH EXISTING DCSS OF THE HYBRID MG

Category		PM in [13]	DDC in [14]	DAPI in [20]	DAPI in [21]	DCC in [22]	PTC in [24]	DMPC in [25]	ET-DMFAC
Power sharing	Accurate	Low	Low	Low	High	High	High	High	High
	Global	×	×	√	×	√	√	√	√
	Proportional	×	×	√	×	√	√	√	√
Voltage/Frequency restoration		×	×	√	√	×	√	√	√
Trigger modes		None	None	Time	Time	Time	Time	Time	Event
Communication burden		None	None	High	High	High	High	High	Low
Controller		Linear	Adaptive	Linear	Linear	Linear	Finite time	MPC	Adaptive
Controller design		Simple	Simple	Simple	Simple	Simple	Complex	Complex	Simple

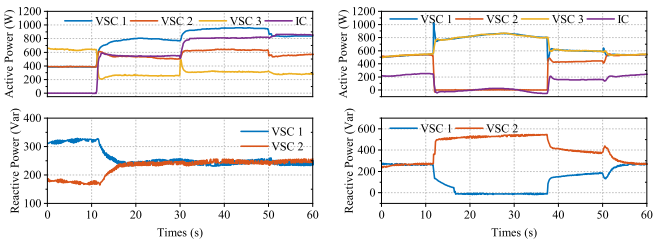

Fig. 5. Experiment results. (a) Proportional power sharing. (b) VSC2 plug and play.

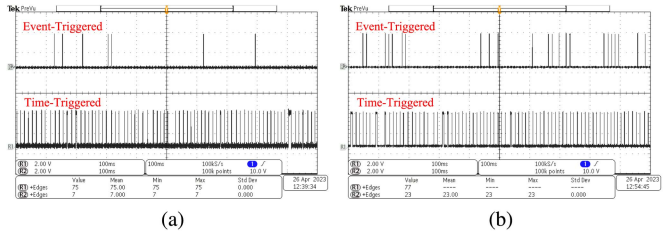

Fig. 6. Trigger time under different trigger modes. (a) Active control. (b) Reactive control.

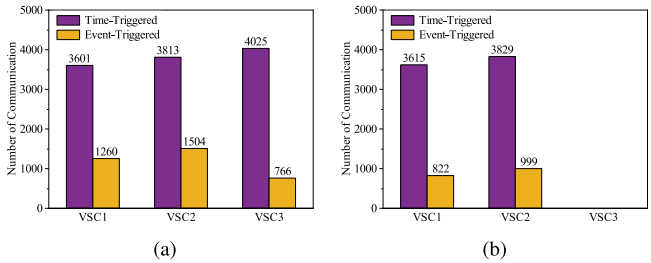

Fig. 7. Number of communications during the experiment. (a) Active control. (b) Reactive control.

the ac-MG being transferred to VSC1. Consequently, there is an overshoot in the output power of VSC1. After $t = 30$ s, VSC2 works in a synchronized mode and goes into operation at about $t = 37$ s. Then, at $t = 50$ s, VSC2 accesses the communication network and shares the load with other DGs. It is evident that power sharing is realized among the remaining VSCs when some VSCs quit operation. After restart, the reaccessed VSC obtains the power reference by negotiating with the already existing VSCs through the proposed strategy, and power is shared again among all the VSCs.

D. Comparison

Comprehensive comparisons with the state-of-the-art DCSs in the hybrid ac/dc MG have been illustrated in Table IV, including power management (PM) [13], data-driven control (DDC) [14], distributed averaged proportional–integral (DAPI) [20], [21], distributed coordination control (DCC) [22], predefined-time control (PTC) [24], and distributed model predictive control (DMPC) [25]. It is evident that the proposed ET-DMFAC provides comprehensive solutions and advantages with respect to communication efficiency and system design simplicity. In order to highlight the performance of the proposed ET-DMFAC, several experiments for comparison have been conducted considering different working conditions, such as trigger modes and droop slopes.

1) Different Trigger Modes: The trigger time in different modes (ET and time-triggered) is shown in Fig. 6. In the time-triggered mode, communication is activated within a predefined period. The trigger time is continuous and evenly spaced. In contrast, only several triggers take effect in the ET-DMFAC. Thus, the communication burden of the DCS can be relieved. Herein, an experiment following the same process of Section IV-B is conducted, and the number of communications for different VSCs is shown in Fig. 7. The ET mode simply reduces the communication by two-thirds, resulting in a significant reduction of the communication burden.

2) Different Droop Slope: To demonstrate the adaptive regulation ability of the ET-DMFAC, an experiment is designed to compare the proposed ET-DMFAC with the DAPI controller in [20] under different droop slopes of VSC3. The results are shown in Fig. 8. The droop slope changes three times at $t = 25$, $t = 40$, and $t = 50$ s, respectively. In Fig. 8(a), accurate power sharing cannot be guaranteed by using the DAPI controller. There is a slight oscillation of the dc current of VSC3, as shown in Fig. 8(b). Since a linear controller is used in the DAPI method where the parameters are designed at a specific operating point, the control performance deteriorates with the increase of droop slope. However, the proposed ET-DMFAC is much

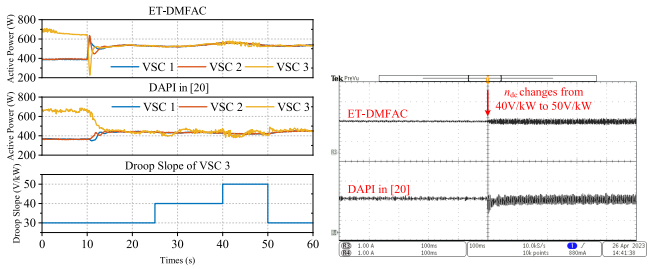

(a) (b)

Fig. 8. Experiment results under different droop slopes of VSC3. (a) Active power. (b) DC current of VSC3.

more adaptive and keeps robustness under different working conditions.

V. Conclusion

This article proposed an ET-DMFAC strategy to achieve global power sharing and frequency/voltage restoration of a hybrid ac/dc MG. The control strategy could operate in a unified control framework and realize the control objectives in a distributed manner. The theoretical analysis showed that asymptotic stability could be guaranteed with the predefined ET mechanism. The experimental results showed that the proposed strategy could maintain a high level of control performance under different operating conditions, such as step change of load and increase of droop slope, and achieve the plug-and-play capability of partial DGs. In addition, two-thirds of the communication links could be reduced by using the ET mechanism. Future work will focus on the power sharing of the hybrid ac/dc MG under an unbalanced and nonlinear load.

Appendix

A. Proof of Lemma 1

According to the definition of substochastic matrix, entry of the matrix $M \in \mathbb{R}^{N\times N}$ satisfies the following conditions:

$$\begin{cases} m_{ij} > 0 \quad \forall i,j \in [1,N] \\ \sum_{j=1}^{N} m_{ij} < 1 \quad \forall i \in [1,N]. \end{cases} \tag{29}$$

According to (29), the 1-norm of the matrix M satisfies $\|M\|_1 < 1$.

Because the matrix M is symmetrical, the 2-norm of M is equal to its spectral radius $\rho_r(M)$. Considering the relationship between the spectral radius and the induced norm, the following inequality holds:

$$\|M\|_2 = \rho_r(M) \le \|M\|_1 < 1 \tag{30}$$

$\forall x \in \mathbb{R}^N$, the quadratic form of $I - M^T M$ can be expressed in (31) by combining the inequality $\|Mx\|_2 \le \|M\|_2 \|x\|_2$ as

$$x^T(I - M^T M)x = \|x\|_2 - \|Mx\|_2 \ge (1 - \|M\|_2)\|x\|_2 > 0. \tag{31}$$

Therefore, the matrix $I - M^T M$ is positive definite and its all eigenvalues satisfy $\lambda(I - M^T M) > 0$. ■

B. Proof of Lemma 2

Let $x_1, x_2, \ldots, x_N \in \mathbb{R}^N$ be the N orthonormal eigenvectors of M. These vectors are linearly independent and satisfy the following equation:

$$\begin{cases} x_j^T x_i = 0, \ i \ne j \\ x_j^T x_i = 1, \ i = j \end{cases} \tag{32}$$

$\forall x \in \mathbb{R}^N$, the vector x can be expressed as $x = \sum_{i=1}^{N} k_i x_i$. Then, the quadratic form of M can be denoted as

$$\begin{aligned} x^T M x &= \left(\sum_{i=1}^{N} k_i x_i^T\right) M \left(\sum_{i=1}^{N} k_i x_i\right) \\ &= \left(\sum_{i=1}^{N} k_i x_i^T\right)\left(\sum_{i=1}^{N} \lambda_i k_i x_i\right) \\ &= \sum_{i=1}^{N}\sum_{j=1}^{N} \lambda_i k_i k_j x_j^T x_i = \sum_{i=1}^{N} \lambda_i k_i^2 \ge \lambda_{\min} \sum_{i=1}^{N} k_i^2 \\ &= \lambda_{\min} x^T x \end{aligned} \tag{33}$$

where λ_i is the ith eigenvalue of M and $\lambda_{\min}$ is the minimum value of λ_i.

According to (33), the inequality $\lambda_{\min} x^T x \le x^T M x$ can be obtained. ■

References

[1] J. Choi, S. I. Habibi, and A. Bidram, "Distributed finite-time event-triggered frequency and voltage control of AC microgrids," *IEEE Trans. Power Syst.*, vol. 37, no. 3, pp. 1979–1994, May 2022.

[2] J. M. Guerrero, J. C. Vasquez, J. Matas, L. G. De Vicuna, and M. Castilla, "Hierarchical control of droop-controlled AC and DC microgrids—A general approach toward standardization," *IEEE Trans. Ind. Electron.*, vol. 58, no. 1, pp. 158–172, Jan. 2011.

[3] R. Wang, D. Ma, M.-J. Li, Q. Sun, H. Zhang, and P. Wang, "Accurate current sharing and voltage regulation in hybrid wind/solar systems: An adaptive dynamic programming approach," *IEEE Trans. Consum. Electron.*, vol. 68, no. 3, pp. 261–272, Aug. 2022.

[4] J. W. Simpson-Porco, Q. Shafiee, F. Dörfler, J. C. Vasquez, J. M. Guerrero, and F. Bullo, "Secondary frequency and voltage control of Islanded microgrids via distributed averaging," *IEEE Trans. Ind. Electron.*, vol. 62, no. 11, pp. 7025–7038, Nov. 2015.

[5] W. Gu, G. Lou, W. Tan, and X. Yuan, "A nonlinear state estimator-based decentralized secondary voltage control scheme for autonomous microgrids," *IEEE Trans. Power Syst.*, vol. 32, no. 6, pp. 4794–4804, Nov. 2017.

[6] A. Milczarek, M. Malinowski, and J. M. Guerrero, "Reactive power management in islanded microgrid—Proportional power sharing in hierarchical droop control," *IEEE Trans. Smart Grid*, vol. 6, no. 4, pp. 1631–1638, Jul. 2015.

[7] Y. Han, P. Shen, X. Zhao, and J. M. Guerrero, "An enhanced power sharing scheme for voltage unbalance and harmonics compensation in an islanded AC microgrid," *IEEE Trans. Energy Convers.*, vol. 31, no. 3, pp. 1037–1050, Sep. 2016.

[8] S. Peyghami, H. Mokhtari, P. Davari, P. C. Loh, and F. Blaabjerg, "On secondary control approaches for voltage regulation in DC microgrids," *IEEE Trans. Ind. Appl.*, vol. 53, no. 5, pp. 4855–4862, Sep./Oct. 2017.

[9] A. Tah and D. Das, "An enhanced droop control method for accurate load sharing and voltage improvement of isolated and interconnected DC microgrids," *IEEE Trans. Sustain. Energy*, vol. 7, no. 3, pp. 1194–1204, Jul. 2016.

[10] Y. Li, Z. Zhang, T. Dragicevic, and J. Rodriguez, "A unified distributed cooperative control of DC microgrids using consensus protocol," *IEEE Trans. Smart Grid*, vol. 12, no. 3, pp. 1880–1892, May 2021.

[11] V. Nasirian, S. Moayedi, A. Davoudi, and F. L. Lewis, "Distributed cooperative control of DC microgrids," *IEEE Trans. Power Electron.*, vol. 30, no. 4, pp. 2288–2303, Apr. 2015.

[12] S. K. Sahoo, A. K. Sinha, and N. K. Kishore, "Control techniques in AC, DC, and hybrid AC–DC microgrid: A review," *IEEE Trans. Emerg. Sel. Topics Power Electron.*, vol. 6, no. 2, pp. 738–759, Jun. 2018.
[13] N. Eghtedarpour and E. Farjah, "Power control and management in a hybrid AC/DC microgrid," *IEEE Trans. Smart Grid*, vol. 5, no. 3, pp. 1494–1505, May 2014.
[14] H. Zhang, J. Zhou, Q. Sun, J. M. Guerrero, and D. Ma, "Data-driven control for interlinked AC/DC microgrids via model-free adaptive control and dual-droop control," *IEEE Trans. Smart Grid*, vol. 8, no. 2, pp. 557–571, Mar. 2017.
[15] Y. Xia, W. Wei, M. Yu, X. Wang, and Y. Peng, "Power management for a hybrid AC/DC microgrid with multiple subgrids," *IEEE Trans. Power Electron.*, vol. 33, no. 4, pp. 3520–3533, Apr. 2018.
[16] P. Yang, Y. Xia, M. Yu, W. Wei, and Y. Peng, "A decentralized coordination control method for parallel bidirectional power converters in a hybrid AC–DC microgrid," *IEEE Trans. Ind. Electron.*, vol. 65, no. 8, pp. 6217–6228, Aug. 2018.
[17] X. Liu, P. Wang, and P. C. Loh, "A hybrid AC/DC microgrid and its coordination control," *IEEE Trans. Smart Grid*, vol. 2, no. 2, pp. 278–286, Jun. 2011.
[18] X. Lu, J. M. Guerrero, K. Sun, J. C. Vasquez, R. Teodorescu, and L. Huang, "Hierarchical control of parallel AC-DC converter interfaces for hybrid microgrids," *IEEE Trans. Smart Grid*, vol. 5, no. 2, pp. 683–692, Mar. 2014.
[19] M. Hosseinzadeh and F. R. Salmasi, "Power management of an isolated hybrid AC/DC micro-grid with fuzzy control of battery banks," *IET Renew. Power Gener.*, vol. 9, no. 5, pp. 484–493, 2015.
[20] E. Espina, R. Cárdenas-Dobson, J. W. Simpson-Porco, D. Sáez, and M. Kazerani, "A consensus-based secondary control strategy for hybrid AC/DC microgrids with experimental validation," *IEEE Trans. Power Electron.*, vol. 36, no. 5, pp. 5971–5984, May 2021.
[21] H. Yoo, T. Nguyen, and H. Kim, "Consensus-based distributed coordination control of hybrid AC/DC microgrids," *IEEE Trans. Sustain. Energy*, vol. 11, no. 2, pp. 629–639, Apr. 2020.
[22] K. Zhang, M. Su, Z. Liu, H. Han, X. Zhang, and P. Wang, "A distributed coordination control for islanded hybrid AC/DC microgrid," *IEEE Syst. J.*, vol. 17, no. 2, pp. 1819–1830, Jun. 2023.
[23] J. J. Wang, C. Y. Dong, C. Jin, P. F. Lin, and P. Wang, "Distributed uniform control for parallel bidirectional interlinking converters for resilient operation of hybrid AC/DC microgrid," *IEEE Trans. Sustain. Energy*, vol. 13, no. 1, pp. 3–13, Jan. 2022.
[24] Y. Zhang, Y. W. Wang, X. K. Liu, W. Yang, and S. M. Liang, "Distributed predefined-time control for hybrid AC/DC microgrid," *IEEE Trans. Ind. Electron.*, vol. 70, no. 8, pp. 8324–8333, Aug. 2023.
[25] E. Rute-Luengo et al., "Distributed model-based predictive secondary control for hybrid AC/DC microgrids," *IEEE Trans. Emerg. Sel. Topics Power Electron.*, vol. 11, no. 1, pp. 627–642, Feb. 2023.
[26] J. Lu, B. Zhang, X. Hou, and J. M. Guerrero, "A distributed control strategy for unbalanced voltage compensation in islanded AC microgrids without continuous communication," *IEEE Trans. Ind. Electron.*, vol. 70, no. 3, pp. 2628–2638, Mar. 2023.
[27] Z. Li, Z. Cheng, J. Si, and S. Li, "Distributed event-triggered hierarchical control to improve economic operation of hybrid AC/DC microgrids," *IEEE Trans. Power Syst.*, vol. 37, no. 5, pp. 3653–3668, Sep. 2022.
[28] T. Dragičević, "Model predictive control of power converters for robust and fast operation of AC microgrids," *IEEE Trans. Power Electron.*, vol. 33, no. 7, pp. 6304–6317, Jul. 2018.
[29] Z. Ma, Z. Wang, Y. Guo, Y. Yuan, and H. Chen, "Nonlinear multiple models adaptive secondary voltage control of microgrids," *IEEE Trans. Smart Grid*, vol. 12, no. 1, pp. 227–238, Jan. 2021.
[30] Z. Hou and S. Jin, *Model Free Adaptive Control: Theory and Applications*. Boca Raton, FL, USA: CRC Press, 2013.
[31] X. Wu, S. Xu, X. Shi, M. Shahidehpour, M. Wang, and Z. Li, "Mitigating subsynchronous oscillation using model-free adaptive control of DFIGs," *IEEE Trans. Sustain. Energy*, vol. 14, no. 1, pp. 242–253, Jan. 2023.
[32] Z. Hou and S. Jin, "A novel data-driven control approach for a class of discrete-time nonlinear systems," *IEEE Trans. Control Syst. Technol.*, vol. 19, no. 6, pp. 1549–1558, Nov. 2011.
[33] J. S. Gómez, D. Sáez, J. W. Simpson-Porco, and R. Cárdenas, "Distributed predictive control for frequency and voltage regulation in microgrids," *IEEE Trans. Smart Grid*, vol. 11, no. 2, pp. 1319–1329, Mar. 2020.

Chang Yang (Student Member, IEEE) received the B.S. and M.S. degrees in 2018 and 2021, respectively, in electrical engineering from the School of Electrical Engineering, Xi'an Jiaotong University, Xi'an, China, where he is currently working toward the Ph.D. degree in electrical engineering.

His current research interests include control and protection of microgrid, renewable energy, and distributed and model-free control.

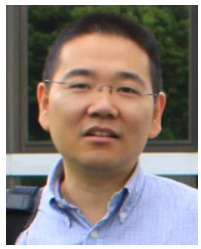

Tao Zheng received the B.S., M.S., and Ph.D. degrees in electrical engineering from the School of Electrical Engineering, Xi'an Jiaotong University, Xi'an, China, in 1999, 2003, and 2007, respectively.

He is currently an Associate Professor with Xi'an Jiaotong University. His current research interests include power system communications, distribution network fault location, and microgrid control and protection.

Ming Bu received the B.S. degree in electrical engineering from the School of Electrical Engineering, Xi'an Jiaotong University, Xi'an, China, in 2022, where she is currently working toward the M.S. degree in electrical engineering.

Her main research focuses on coordination control of energy router.

Pengyu Li received the B.S. degree in 2021, in electrical engineering, from the School of Electrical Engineering, Xi'an Jiaotong University, Xi'an, China, where he is currently working toward the M.S. degree in electrical engineering.

His current research focuses on the application of advanced control strategy on microgrid, such as the sliding mode control and fuzzy PID.

Josep M. Guerrero (Fellow, IEEE) received the B.S. degree in telecommunications engineering, the M.S. degree in electronics engineering, and the Ph.D. degree in power electronics from the Technical University of Catalonia, Barcelona, Spain, in 1997, 2000, and 2003, respectively.

Since 2011, he is a Full Professor with the Department of Energy Technology, Aalborg University, Aalborg, Denmark, where he is responsible for the Microgrid Research Program. From 2012, he is a Guest Professor with the Chinese Academy of Science and the Nanjing University of Aeronautics and Astronautics, Nanjing, China, and since 2014, he is a Chair Professor with Shandong University, Shandong, China. His research focuses on different microgrid aspects, including power electronics, distributed energy-storage systems, hierarchical and cooperative control, energy management systems, and optimization of microgrids and islanded minigrids.

Dr. Guerrero is an Associate Editor for several IEEE Transactions journals.